Diagnosis of Diabetic Retinopathy by Extracting Blood Vessels and Exudates using Retinal Color Fundus Images

G.S.ANNIE GRACE VIMALA[1] AND S.KAJAMOHIDEEN[2]

[1]Associate professor, [2]Professor
Department of Electronics and Communication Engineering,
B.S.Abdur Rahman University,
Chennai, India

Email: gsannie77@gmail.com[1]

Abstract: - Diabetic retinopathy (DR) is the damage caused by complications of diabetes to the retina. It is one of the leading causes of blindness across the world. Hence, an accurate, premature diagnosis of DR is an essential task because of its potentiality for reducing the number of cases of blindness across the globe. The main objective of our study was to develop a cost-effective computer-aided diagnostic system (CAD) in order to evaluate the performance of the system which automatically classifies images with pathologic features commonly found in DR. This study was performed on 60 South Indian subjects whose age ranged from 50-85 years. For all the subjects, digital images of size 640 x 480 were taken with a CARL ZEISS FF 450 plus Visupac fundus camera. The ground truth results were provided for the presence of pathological conditions such as micro aneurysms, exudates, hemorrhages. An SVM kernel classifier based CAD system was used to report the presence or absence of DR. The next step was the evaluation of the diagnostic capability of the proposed method in order to identify the subjects with DR by means of sensitivity, specificity and accuracy with respect to ground truth results. The proposed system has attained uppermost classification accuracy, reported so far by means of 5-fold cross validation analysis with the average sensitivity, specificity and accuracy values of 91.6%, 90.5% and 91.2% respectively. In conclusion, our findings suggest that the proposed CAD system would be a useful technique for cataloging the subject with DR.

Keywords: Fundus image, blood vessel, image processing, diabetic retinopathy, mathematical morphology, Support Vector Machine

1. Introduction

A direct relativity has been witnessed between proneness to disease and better life expectancy, the aging progression being the mechanism during this sociogramic equation. The diseases, which come into view as a result, are plentiful. To point that, diabetes tops the list, which is a metabolic disease. The quick progression of diabetes is one among the most challenges of the present healthcare industry. The number of individuals affected with the disease continues to rise at a rapid rate. The International Diabetic Federation recently revealed that more than 345 million individuals are suffering from diabetes across the globe [1]. The World Health Organization predicts that the amount of individuals with diabetes will extend from 350 million to 600 million over the next 25 years [2]. Unfortunately, India has the highest number of diabetic patients in the world (i.e. 41 million) [1]. The circumstance is made worse by the very fact that just half of the patients are conscious to the disease and within the medical point of view, diabetes leads to critical problems later. These difficulties include micro and macrovascular transformations that lead to cardiac disorders, renal problems and retinopathy. Approximately 40% of individuals with diabetes have a minimum of gentle signs of diabetic retinopathy [3].

Diabetic retinopathy could be a frequent trouble of diabetes. Indeed, it is thus common that it is the leading reason behind visual defect or blindness

among the working individuals of western countries [4]. Despite of the healthcare state of affairs in their country of the origin, individuals with diabetes are twenty five times more likely to develop visual defect compared with people who do not suffer from the same disease [5]. Diabetic retinopathy could be a silent disease; as a result, it should solely be recognized by the patient once the changes within the retina have progressed to the level wherever treatment is impossible and much complicated. Among patients with diabetes, premature diagnosing and treatment are shown to forestall visual loss and visual defect or blindness [6]–[8]. However, about 50% of the individuals who are suffering from diabetes across the globe do not undergo any type of eye examination [9]. The utilization of digital photography of the retina studied by skilled readers throughout screening programs has been found to be both specific and sensitive in the detection of the premature signs of diabetic retinopathy [10], [11].

Access to screening services is considered as a vital and critical problem, particularly given the increasing prevalence of diabetes. The prevalence of diabetic retinopathy diverges with the age of onset of diabetes and also the time-span of the disease. So far, the most effective treatment for diabetic retinopathy is administered solely in the initial stages of the disease. Hence, early diagnosis through standard screening is of great importance. To extend access to screening, many research teams have proposed the utilization of automatic computer systems for deciding whether the screened individuals ought to be diagnosed by an ophthalmologist or safely come back for screening one year later [9], [12]–[13].These kinds of automatic systems have the potential to cut back the workload for screening ophthalmologists while sustaining a high sensitivity (i.e., higher than 90%) for the diagnosis of individuals with diabetic retinopathy. In order to reduce the cost of such screenings, a digital image acquiring technology ought to be used. This technology permits us to utilize the state-of-the art image processing methods which automate the process of detection of abnormalities in retinal images. Hence, the aim of the present study was to develop a low cost computer aided diagnostic system (CAD) in order to diagnose diabetic retinopathy by extracting blood vessels, optic disk and exudates from retinal digital fundus images.

2. METHODS

2.1 Data description

The present study emphasizes the novel ideas with respect to diabetic retinopathy abnormality within the framework of public health. A free eye screening camp was conducted in a leading eye care hospital, Chennai, India, at the end of the year 2012. This study was performed on 60 South Indian subjects whose age ranged from 50- 85 years. Prior to the study, a detailed questionnaire was filled in by the patients, signed and informed consent form to the investigation protocol.For all the subjects, digital images of size 640 x 480 were taken with a CARL ZEISS FF 450 plus Visupac fundus camera.

2.2 Fundus image analysis

The retina is a layered structure with numerous layers of neurons interconnected by synapses and is a light-sensitive tissue lining the internal surface of the eye. The central retinal artery and vein seems available to one another at the nasal side of the middle of the optic disk [14]. Information regarding the structure of blood vessels can assist in categorizing the cruelty of diseases and can conjointly assist as a landmark throughout the segmentation process. Distinct features of the fundus image are displayed in Figure 1.

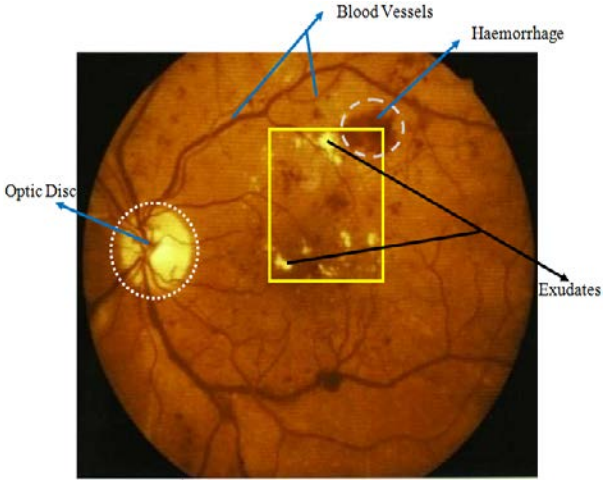

Fig. 1 A sample fundus image with different features

Accumulations of protein and lipid in the retina are called Exudates. Naturally, they are white or cream colored, reflective and bright lesions witnessed on the retina. They signify exaggerated vessel permeability and its related risk of retinal edema or swelling. A vital step with in the extraction framework is

removing distinguished structures of the retina, such as blood vessel tree and optic disc. After these structures have been removed, the exudates candidates are detected and highlighted.

2.2.1 Color normalization

The pigmentation in the retinal tissue widely varies across the patients. Hence the color of exudates may not seem brighter than the background in some regions of the image. Thus the images were normalized to a standard reference image selected from the test data set by means of histogram specification techniques. Initially, histogram equalization was performed for each sub channel of the RGB image by Global-local adaptive histogram equalization using partially-overlapped windows (GLAPOW) method [15], followed by intensity normalization step using histogram specification. This modifies the image values through a histogram transformation operator which maps a given intensity distribution L(x, y) into a desired distribution N(x, y) using a histogram equalized image M(x, y) as an intermediate stage. This process was applied independently to each individual sub blocks of 5 x 5 [16].

After normalization, a local contrast enhancement method was applied to improve both the contrasting attribute of tissue pigments and the overall intensity in the image. The aim was to apply a transformation of the values inside small windows in the image in a way that all values were distributed around the mean and showed all possible intensities [16], [17]. Hence, given each pixel in the initial image and a small running window then the image was filtered to produce the new image (I) based on Eq.1.

$$I(x,y) = N * \left[\frac{\Phi_w(p) - \Phi_w(\min)}{\Phi_w(\max) - \Phi_w(\min)} \right] \qquad (1)$$

Where N is the peak signal, *p* is intensity of the pixel and Φ_w is sigmoid function as well as max and min refers whole image maximum and minimum values respectively. Finally, color normalization was accomplished by merging the normalized R, G, B components and it is shown in the Figure 2.

2.2.2 Edge enhancement

In the next phase, Kirsch's template [14] was utilised for identifying the blood vessels from the normalized color images. For detecting the edges, the operator made use of eight templates, which were successively rotated by 45° as shown in Figure 3.

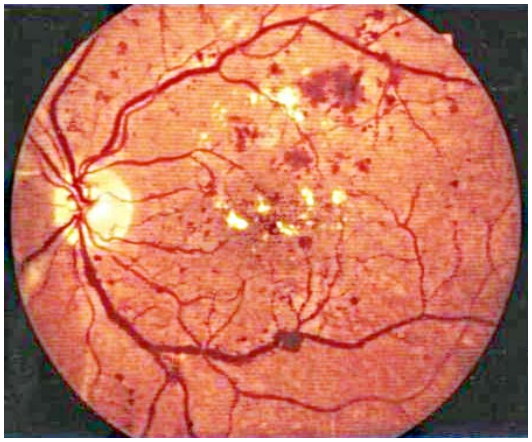

Fig 2. Normalized color image

0°			45°			90°			135°		
5	-3	-3	-3	-3	-3	-3	-3	-3	-3	-3	-3
5	0	-3	5	0	-3	-3	0	-3	-3	0	5
5	-3	-3	5	5	-3	5	5	5	-3	5	5
180°			**225°**			**270°**			**315°**		
-3	-3	5	-3	5	5	5	5	5	5	5	-3
-3	0	5	-3	0	5	-3	0	-3	5	0	-3
-3	-3	5	-3	-3	-3	-3	-3	-3	-3	-3	-3

Fig 3. Templates of Kirsch's method

The gradient was then computed by convolving the normalized image with eight template impulse response arrays in each and every pixel. Thus, the gradient of different directions was achieved and the final gradient was the summation of the enhanced edges by considering all directions for RGB channel than any one specific channel and shown in Figure 4.

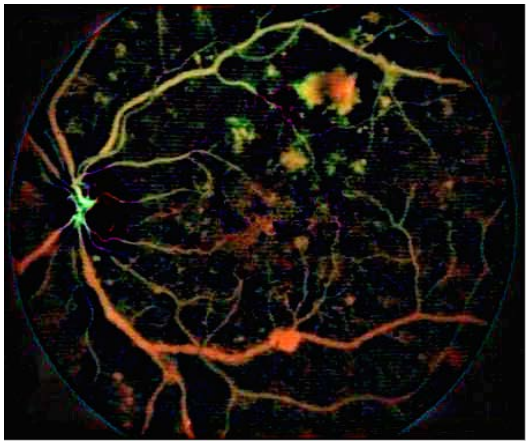

Fig 4. Enhanced image by Kirsch's method

2.2.3 Color space conversion

In the next step, the enhanced RGB color images were converted in to HSV color image using the Eq. (2).

$$\left.\begin{aligned} H &= \begin{cases} \theta, if\ B \le G \\ 360-\theta, if\ B > G \end{cases} \\ S &= 1-\left\{\frac{3}{R+G+B}\right\}\min(R,G,B) \\ I &= \frac{(R+G+B)}{3} \end{aligned}\right\} \quad (2)$$

Where,

$$\theta = \cos^{-1}\left\{\frac{\left[(R-G)+(R+B)\right]}{\left[(R-G)^2+(R-B)(G-B)\right]^{\frac{1}{2}}}\right\} \quad (3)$$

Min(*R, G, and B*) denotes the minimum value among of red, green and blue components of the image [18].

Then the intensity channel of the HSV image alone was extracted and displayed in Figure 5. Here, the intensity level between the blood vessels (foregrounds) was comparatively low with other background regions. Hence, selecting an accurate threshold value to segment the objects of interest is a tough task. So, the subsequent enhancement of the image for further analysis seems to be essential. Therefore, in the subsequent step, a spatial averaging filter of size 13 × 13 was applied to the gray scale (i.e. intensity channel) image and shown in Figure 6. The obtained image was then equalized by performing histogram equalization in order to obtain the gray levels in the range [0, L−1] and displayed in Figure 7.

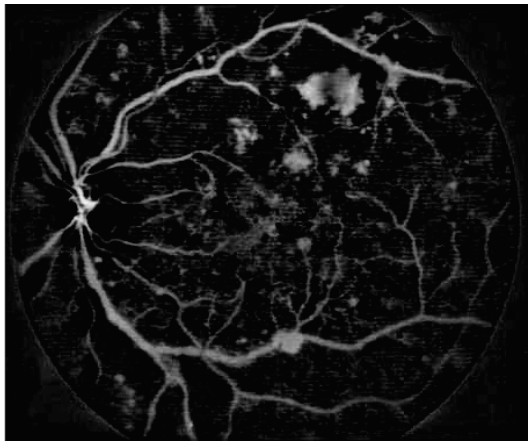

Fig 5. Intensity channel image of enhanced edge by Kirsch's method

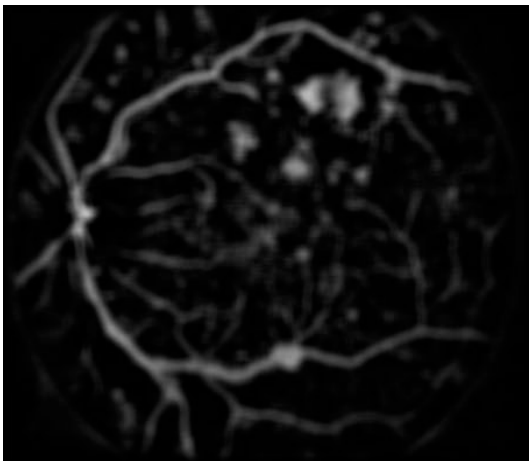

Fig 6. Spatial averaging filtered image

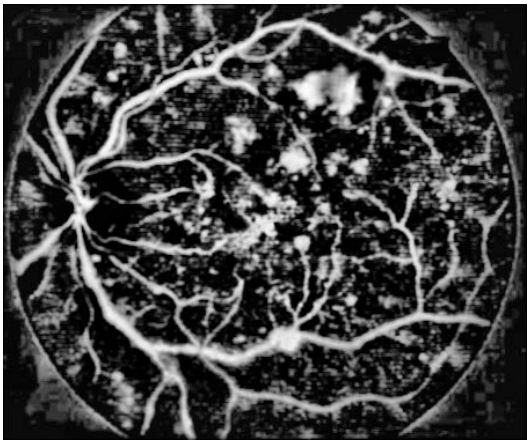

Fig 7. Histogram equalized image

2.2.4 Binarization

In the next step, binarization process was done by setting a heuristic threshold value (T = 0.78). The adopted threshold value was efficient and found very appropriate for our test image data set. This process would result in two sets of pixels, as exemplified in Eq. (4) and the resultant image is shown in Figure 8.

$$I_B(x,y) = \begin{cases} 1(\text{white}), & \text{if } I(x,y) \ge T \\ 0(\text{black}), & \text{otherwise} \end{cases} \quad (4)$$

Then the morphological closing process is essential in order to close the holes or unfilled area within the blood vessel region [19] and the outcome is shown in Figure 9.

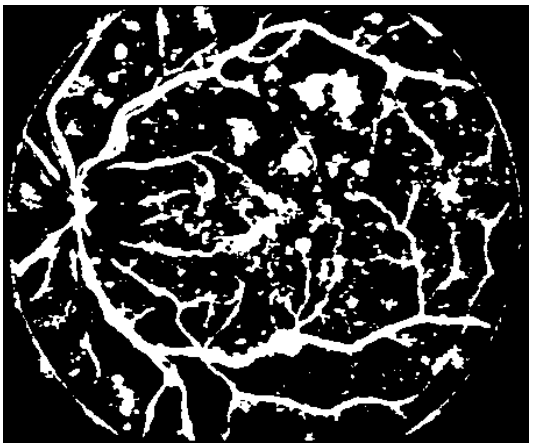

Fig 8. Binarized image

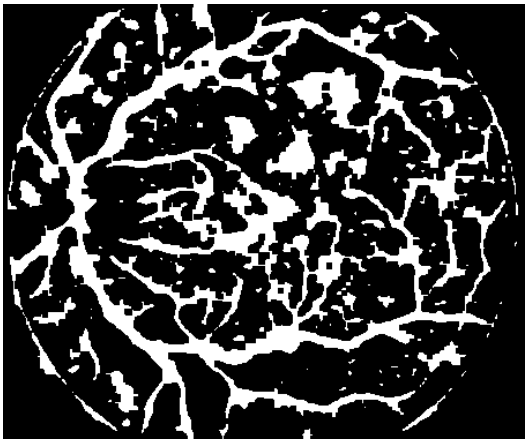

Fig 9. Morphological holes filled binary image

2.2.5 Feature extraction

The binary image contains many objects such as blood vessels, optic disc, exudates, etc., in the retinal region. In order to retain only exudates contents (smaller objects) in the binary image (I_B) following steps were carried out.

(1) The blood vessels contain no information about exudates. Hence, the technique detailed by Badsha et al [20] was used to extract only blood vessels shown in Figure 7 and remove them from the obtained binary image (I_B).

(2) Optic disc is the most apparent feature (the brightest area that can be observed as a pale, well-defined round or vertically somewhat oval) in a fundus image, which is the entrance region of blood vessels and optic nerve to the retina and serves as the locus of most other features. Thus, in order to remove the optic disc from binary image (I_B) the methodology prescribed by Valencia et al [21] was utilized.

(3) Finally, to remove the border of the retina from the binary image (I_B) the following equation (Eq.5) was applied [22], [23] and the resultant image is shown in Figure 10.

$$I_E(x,y) = \begin{Bmatrix} I_B(x,y), (x,y) \in \text{border of } I \\ 0, \quad \text{otherwise} \end{Bmatrix} \qquad (5)$$

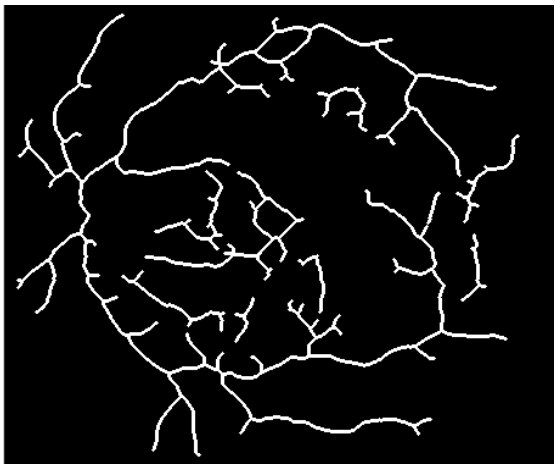

Fig 10 Extracted vessels image

The following morphological features detailed by Sopharak et al [24], [25] were extracted from the image (I_B - I_E) which contains only small objects information:

i. ***Area:*** The area was calculated based on total number of white pixels with black pixel as the neighbor in the binary image.

ii. ***Number of regions:*** Number of regions is nothing but the total number of segments in the binary image.

iii. ***Eccentricity:*** Eccentricity was estimated based on major and minor axis lengths respectively by using the following equation:

$$\text{Eccentricity} = \frac{1}{L_1}\sqrt{\left(L_1^2 - L_2^2\right)} \qquad (6)$$

Where L_1 and L_2 are major and minor axis lengths respectively.

iv. ***Extent:***

$$\text{Extent} = \frac{\text{Area}}{\text{Area of bounding box}} \tag{7}$$

v. ***Orientation:*** Orientation is defined as the angle between major axis of the segmented object that has the same second moments around the region and the horizontal axis.

vi. ***Convex area of the polygon:*** Convex polygon area consisting of a segmented region is given by

$$\text{Convex area} = \frac{1}{2}\begin{bmatrix} x_1 & y_1 \\ \vdots & \vdots \\ x_n & y_n \\ x_1 & y_1 \end{bmatrix} = \frac{1}{2}\begin{bmatrix} \left(x_1.y_2 + x_2.y_3 + x_3.y_4 + \cdots + x_n.y_1\right) \\ -\left(y_1.x_2 + y_2.x_3 + y_3.x_4 + \cdots + y_n.x_1\right) \end{bmatrix} \tag{8}$$

The starting and ending point of the coordinates should be arranged in counter clockwise direction around the polygon.

vii. ***Solidity:*** Solidity could be defined as the ratio of the solid or filled area and convex hull area i.e.

$$\text{Solidity} = \frac{\text{Filled Area}}{\text{Convex area}} \tag{9}$$

2.3 Classification

A kernel-based SVM has been adopted to check the enforcement of the present diagnosis system in order to attain high accuracy [26–28]. RBF was utilized as the kernel function as it was evidenced to work well on our datasets. Optimization of the parameter combination was sought by quadratic programming and found to have yielded better categorization outputs at $\gamma = 1$ and $C = 1$. Small values were used with the intention of keeping reproducing noise and over-fitting at bay to the data samples that were used in the training procedure. By performing investigation on the training samples, it was possible to actuate the RBF parameter and weighting factors. A data analysis scheme written in MATLAB was excavated, which makes use of existing SVM tools for MATLAB that were actualized by Scholkopf [29] to perform classification.

3. RESULTS

Outcomes of the classifier were compared with the ophthalmologists' hand-drawn ground-truth images in order to evaluate the performance of the proposed technique. Typically, the performance of the DR identification systems is evaluated with Sensitivity, Specificity and Accuracy. Keeping this factor in view, the confusion matrix has been designed, taking into consideration, the trade-off between the actual and classifier generated outputs as shown in Table 1.

Table 1. Alternative diagnostic test (classifier) results with respect to the ground-truth outcome

Diagnostic tool (classifier) result	Ground-truth result (ophthalmologists' hand-drawn)	
	Positive (present)	Negative (absent)
Positive	TP	FP
Negative	FN	TN

True positive (TP) is defined as the fact in which the subject would be predicted to possess DR, when actually it is the case. True negative (TN) is the process in which subject would be predicted as normal and also the subject would possess normal health in reality. Similarly, false positive (FP) is the condition of incorrect DR prediction when the subject would be normal in reality. False negative (FN) is a condition which is normal prediction, when the person is DR in reality.

The sensitivity measures the proportion of actual positives which are correctly identified as such (e.g. the percentage of DR people who are identified as having the DR). The sensitivity of the test indicates the probability that it would indicate a TP result when used on an infected subject. The sensitivity of the test could be determined by the formula.

$$\text{Sensitivity} = \frac{\text{TP}}{\left(\text{TP} + \text{FN}\right)} \text{X}\, 100 \tag{10}$$

The specificity measures the proportion of negatives, which are correctly identified (e.g. the percentage of healthy people who are identified as not having the DR). A theoretical optimal prediction could achieve 100% sensitivity (i.e. predict all people from the DR group as DR) and 100% specificity. The

specificity of a test is the probability that a test would produce a TN result when used on a non-infected population. The specificity of a test could be determined by calculating:

$$\text{Specificity} = \frac{\text{TN}}{(\text{TN} + \text{FP})} \text{X}\,100 \qquad (11)$$

The Accuracy of the test indicates the closeness of the test results to the true value and repeatability of the test. The accuracy of the test could be determined by the formula:

$$\text{Accuracy} = \frac{(\text{TP} + \text{TN})}{(\text{TP} + \text{TN} + \text{FP} + \text{FN})} \text{X}\,100 \qquad (12)$$

A set of 60 retinal digital fundus images including 34 (57%) images with exudates and 26 (43%) images without exudates were tested on an Intel E7500 Core2Duo processor, 2.93 GHz PC using MATLAB. The feature extraction techniques detailed in the methodology section (eq.6 to eq.9) were applied to the each of the fundus images and 7 features were extracted and stored. Then the classification process of the images was performed based on RBF-kernel SVM. For the SVM classifier, 32 images were utilized for training the classifier and 28 images for testing the classifier in each fold of analysis.

Table 2 gives information based on the 5-fold cross validation as regards to average percentage of 92% sensitivity and 91% specificity of the diagnostic classification based on the predictions of the RBF kernel-SVM within the framework of ground-truth outcomes. Finally, the proposed SVM based CAD system produced 91% accuracy in the classification of DR.

Table 2. Performance of the SVM classifier via 5-fold cross validation

	Sensitivity (%)	**Specificity (%)**	**Accuracy (%)**
Fold ≠1	94.1	90.9	92.8
Fold ≠2	87.5	89.3	85.7
Fold ≠3	94.7	88.9	97.7
Fold ≠4	92.3	89.6	89.2
Fold ≠5	85.7	92.9	89.5
Average	**91.6**	**90.5**	**91.2**

The final resulting image of exudates detection from SVM classification method is shown in the following figure (Figure 11):

Fig 11. Super imposed exudates on the input image

4. DISCUSSION

Even though it is promising to prevent from vision loss by premature diagnosis and appropriate management of DR, lack of urgency and appropriate healthcare with regard to routine eye examination, additionally poor access to DR screening programs could leave several diabetic patients, who have developed DR, to continue being unknown and untreated. The assessment of the quality of pathology detection is a complex task; human visual grading systems are not always perfect. Consequently, if a human grader does not agree with the automated detection algorithm, this could be due to either an error of the human visual grading or due to an error of the detection algorithm.

The proposed CAD system based on SVM classifier is advantageous on account of its simple protocol and wide availability of fundus images. This tool is an attempt to screen DR subjects, due to its ability to demonstrate 92% of DR subjects those could be identified properly. Similarly, the findings of Osareh et al also confirm that the SVM classifier achieves a high level of diagnostic accuracy in terms of DR classification over others [30]. Zhang et al studied an automated algorithm using multi-scale morphological processing and it achieved the sensitivity and predictive value of 84.1% and 89.2% respectively [31]. Fleming et al studied multiple linear

top hats by using multi-scale method and it achieved a maximum sensitivity, specificity of 98.6% and 95.5% respectively [32]. The early diagnosis of DR by means of fundus image features accomplished an accuracy of 91.2% and specificity of 92% by SVM classifier.

This proposed CAD system has an edge over manual assessment (ground-truth) by means of automated evaluation. The proposed CAD system, by means of image morphological feature extraction which would reduce the measurement errors, that occur with the conventional (ophthalmologists' hand-drawn) assessments. Although the results of the proposed study are encouraging, more cases of DR are needed for further investigation and validation.

5. CONCLUSION

The development of the proposed CAD system is in progress. The methods to segment anatomical structures such as optic disk, blood vessels and outer border along with exudates were presented and promising results were shown. The proposed CAD system could identify DR cases with an average accuracy of more than 91 %, a sensitivity of more than 91 %, and a specificity of 90.5 %. Therefore, on account of leading satisfied sensitivity, specificity and accuracy results, the proposed methodology is prospected to be a useful technique for cataloging the subject with DR, additionally; it could be supplementary diagnostic methodology that will mask faulty diagnosis.

References

1. The International Diabetes Federation, *Annual report-2012* http://www.idf.org/files/idf_publications/idf_annual_report_2012_EN/index.html#14

2. Danaei G, Finucane MM, Lu Y, Singh GM, Cowan MJ, Paciorek CJ et al. National, regional, and global trends in fasting plasma glucose and diabetes prevalence since 1980: systematic analysis of health examination surveys and epidemiological studies with 370 country-years and 2.7 million participants. *Lancet*, 378(9785):31–40, 2011.

3. Nayak, J., Bhat, P. S., Acharya, U. R., Lim, C. M., and Kagathi,M., Automated identification of different stages of diabetic retinopathy using digital fundus images. J. Med. Syst., USA, 32(2):107–115, 2008.

4. Ong, G. L., Ripley, L. G., Newsom, R. S., Cooper, M., and Casswell, A. G., Screening for sight-threatening diabetic retinopathy: comparison of fundus photography with automated color contrast threshold test. Am. J. Ophthalmol. 137(3):445–452, 2004.

5. Watkins, J. P., ABC of diabetes retinopathy. British Medical Journal 326:924–926, 2003.

6. Kinyoun J, Barton F, Fisher M, Hubbard L, Aiello L, Ferris F,. Detection of diabetic macular edema: ophthalmoscopy versus photography—early treatment diabetic retinopathy study report number 5. The ETDRS research group, *Ophthalmology*. 96:746–750, 1989

7. Early Treatment Diabetic Retinopathy Study Research Group, Early photocoagulation for diabetic retinopathy. ETDRS report 9. *Ophthalmology*.9:766–785, 1991.

8. Bresnick GH, Mukamel DB, Dickinson JC, Cole DR. A screening approach to the surveillance of patients with diabetes for the presence of vision-threatening retinopathy, *Ophthalmology*. 107(1):19 –24, 2000.

9. Abramoff MD, Niemeijer M, Suttorp-Schulten MSA, Viergever MA, Russell SR, van Ginneken B. Evaluation of a system for automatic detection of diabetic retinopathy from color fundus photographs in a large population of patients with diabetes. *Diabetes Care*. 31(2):193–198, 2008.

10. Lin DY, Blumenkranz MS, Brothers RS, Grosvenor DM. The sensitivity and specificity of single-field non-mydriatic monochromatic digital fundus photography with remote image interpretation for diabetic retinopathy screening: A comparison with ophthalmoscopy and standardized mydriatic color photography. *Am. J.Ophthalmol*., 134:204–213, 2002.

11. Williams GA, Scott IU, Haller JA, Maguire AM, Marcus D, McDonald HR. Single-field fundus photography for diabetic retinopathy screening: a report by the American Academy of Ophthalmology. *Ophthalmology*, 111:1055–1062, 2004.

12. Scotland GS, McNamee P, Philip S, et al. Cost-effectiveness of implementing automated grading within the national screening programme for diabetic retinopathy in Scotland. *Br. J.Ophthalmol.*, 91:1518–1523, 2007.

13. Abramoff MD, Reinhardt JM, Russell SR. Automated early detection of diabetic retinopathy. *Ophthalmology*, 117:1147–1154, 2010.

14. Li H, Chutatape O. Fundus Image Feature Extraction. Proc. *Annual EMBS International conference*, pp. 3071–3073, 2000

15. Aibinu AM, Iqbal MI, Nilsson M, and Salami MJE. A New Method of Correcting Uneven Illumination Problem in Fundus Images. *Proc. International Conference on Robotics, Vision, Information, and Signal Processing*, pp. 445-449, 2007.

16. Sapthagirivasan V, Anburajan M, Diagnosis of osteoporosis by extraction of trabecular features from hip radiographs using support vector machine: An investigation panorama with DXA, *Comput. Biol. Med*, Vol. 43(11), pp. 1910–1919, 2013

17. Mahadevan V, Sapthagirivasan V. Information Processing of Medical Images for the Detection of Osteoporosis in Hip Region of Interest. *International Journal of Innovation, Management and Technology*, 1(5):516-520, 2010.

18. Agoston MK. *Computer Graphics and Geometric Modeling: Implementation and Algorithms*. London: Springer, pp. 300–306, 2005.

19. Gonzalez RC, Woods RE, Eddins SL: Digital image processing using MATLAB. Prentice Hall, Upper Saddle River, 2004

20. Badsha S, Reza AW, Tan KG, Dimyati K. A New Blood Vessel Extraction Technique Using Edge Enhancement and Object Classification. *J Digit Imaging*, Springer, 2013

21. Valencia E and Millan MS. Color image analysis of the optic disc to assist diagnosis of glaucoma risk and evolution. *In Proc. of the 3rd IS&T European Conf. on Color in Graphics, Imaging, and Vision*, pp. 298-301, 2006.

22. Reza AW, Eswaran C, Hati S. Diabetic Retinopathy: A Quadtree Based Blood Vessel Detection Algorithm Using RGB Components in Fundus Images. *Journal of Medical Systems*, 32:147–155, 2008

23. Saleh MD, Eswaran C. An efficient algorithm for retinal blood vessel segmentation using h-maxima transform and multilevel thresholding. *Computer Methods in Biomechanics and Biomedical Engineering*, 15(5):517–525, 2012

24. Sopharak A, Uyyanonvara B, Barman S et al. Automatic detection of diabetic retinopathy exudates from non-dilated retinal images using mathematical morphology methods, *Computer Medical Imaging and Graphics*. 32(8):720–727, 2008

25. Morphology Fundamentals: Region and Image Properties: Morphological Operations (Image Processing Toolbox™). http://www.mathworks.in/help/images/ref/regionprops.html (Accessed on August 14, 2013)

26. Vapnik. V. N, the Nature of Statistical Learning Theory, *Springer-Verlag, Berlin Heidelberg*, New York, 1995.

27. Vapnik. V.N, Statistical Learning Theory, *Wiley*, New-York, 1998.

28. Scholkopf. B, Sung. K.K, Burges C.J.C, et. al, Comparing support vector machines with Gaussian kernels to radial basis function classifiers, *IEEE Trans. Signal Process*. 45 (11); 2758–2765, 1997.

29. Scholkopf B, Smola A.J., Learning with Kernels, MIT Press, Cambridge, MA, 2002.

30. Osareh. A, Mirmehdi. M, Thomas. B.T. et al., Comparative Exudates Classification Using Support Vector Machines and Neural Networks, In *Pro. Intl. Conf. Medical Image Computing and Computer-Assisted Intervention-Part II*, Springer-Verlag: London, UK, pp. 413–420, 2002.

31. Zhang. X and Fan. G, Retinal Spot Lesion Detection Using Adaptive Multiscale Morphological Processing, *in Proc. ISVC (2)*, pp.490-501, 2006

32. Fleming AD, Philip S, Goatman KA, et al, Automated detection of blot haemorrhages as a sign of referable diabetic retinopathy, *In: Proc. Medical Image Understanding and Analysis*, 2008.